Institut für
Informations- und Kommunikationstechnologien

ESTEC Contract No. 4000107097/12/NL/AF/fk

Weak GNSS Signal Navigation on the Moon

Executive Summary Report

Submitted by:

JOANNEUM RESEARCH
Forschungsgesellschaft mbH
Leonhardstraße 59

Author(s):

N. Witternigg, G. Obertaxer, M. Schönhuber – JOANNEUM RESEARCH, Austria
G. B. Palmerini, Filippo Rodriguez – DIAEE, La Sapienza, Italy
L. Capponi, C. Mozzetti, B. Buccinnà, N. Borghi – Spacesys s.r.l., Italy
F. Soualle, D. Fernandez–Prim, J-J. Floch – Airbus Defence and Space, Germany

Graz, July 1, 2015

Contents:

Tab. 1 Document History

Version	Modification	Written by	Date
0.1	Initial Version	all	June 2015
0.6	Updated Version	all	July 2015

1 Introduction

In this document some of the key findings and recommendations for a receiver concept using weak GNSS signals for navigation during a Moon mission are summarised. The document contains abbreviated concepts and findings from the MoNav reports D1-D6 which should be used for a more detailed technical reference.

2 Receiver Requirements: Service Volume

The initial step of the analysis is represented by the definition of the GNSS capabilities and receiver requirements in the environment of interest. The service volume concept has been introduced to this aim, and recent studies pointed out the interest to define and include GNSS performance above the altitude of the constellation itself [1], [2]. It is well known that signals, even if primarily broadcast from GNSS sources in order to serve Earth surface and proximity (i.e. with a beam directed nadir), are available at a limited extent also above the constellation. Such a limited availability is mainly due to the spill-over of the beams irradiated from satellites above the other side of the Earth and to secondary lobes (Fig. 1). Due to the distance and/or due to the originally radiated power the received power in such conditions will be indeed low but still exploitable. In fact, a limited service capability will be available to lunar mission with specific characteristics for each possible mission phase.

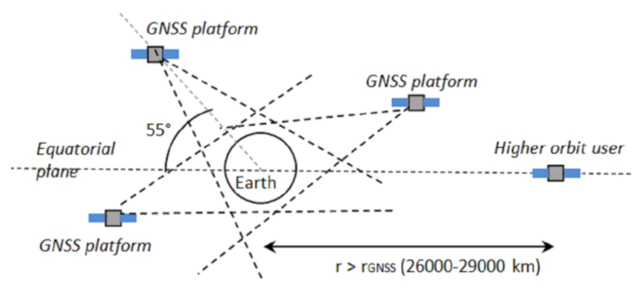

Fig. 1 Spacecraft orbiting at altitudes higher than GNSS constellations are mainly serviced by the spill-over of the signals of far-away satellites positioned at the time above the opposite hemisphere, in addition to secondary lobes of closest GNSS platforms

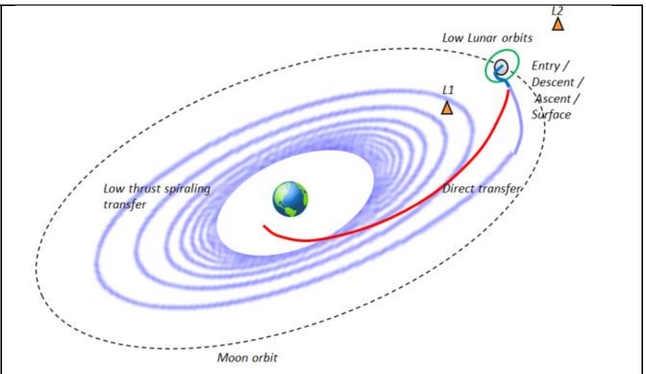

Fig. 2 Different trajectories of interest investigated for GNSS based navigation during Moon exploration

With respect to Earth-Moon transfer, two classes of trajectories can be serviced: (1) classical direct transfer paths with the main portion being defined by a high eccentricity Hohman transfer ellipse [3], and (2) long spiraling trajectories which are carried out by means of continuous low-thrust periods. The latter are becoming especially interesting as they fit the electric propulsion characteristics [4], [5]. We did not analyse extremely low energy transfers, also known as weak stability boundaries' transfers, as they reach distances from Earth of about 10^6 km as part of their cruise where the signal will become too faint [6]. In the lunar entry phase, as well as in ascent/descent and surface exploration, the weak GNSS reception offers the availability of signals with the obvious constraint that those phases should be exploited on the Earth facing side. The very same constraint is intrinsically impossible to satisfy for low lunar orbits, where aiding from different instruments will be mandatory. However, other interesting missions as the ones targeted to the Lagrange point L1 (between Earth and Moon, at approximately 325,000 km from Earth) and L2 (the far away point above the dark side, about 445,000 km from Earth) could benefit from weak - and extremely faint in case of L2 - but definitely available GNSS signals. These two specific conditions are especially appealing to support exploration with the in-orbit assembly of probes bounded to the Moon (L1) and for data relay purposes on the dark side of the Moon (L2). Moreover, these two specific conditions will be granted improved navigation performance thanks to their dynamically steady conditions. Fig. 2 represents the different conditions of interest in the Earth-Moon orbital scenario analysed in the frame of the study, while Fig. 3 clarifies that even the orbit at the Lagrange point L2, partly masked by the Moon ($\sigma \approx 0.9°$, but $\alpha \approx 2.7°$), can achieve the visibility of the GNSS constellation.

A geometrical effect peculiar to lunar missions has been also noticed. GNSS source orbits are ‘anchored’ to the Earth equator, with an inclination of about 55°. The inclination of the orbit of the Moon with respect to the equator is significant, and varies in the range from 18.29° to 28.58° in a 18.6 years period. As a result, the visibility geometry is not perfectly symmetric and there will be a difference - varying in time - in the sources’ visibility from a spacecraft bound to the Moon. Fig. 4 compares the different geometries of GNSS visibility when the Moon (and the approaching spacecraft using GNSS signals) is either at the 'quadrature' or at the 'node' point.

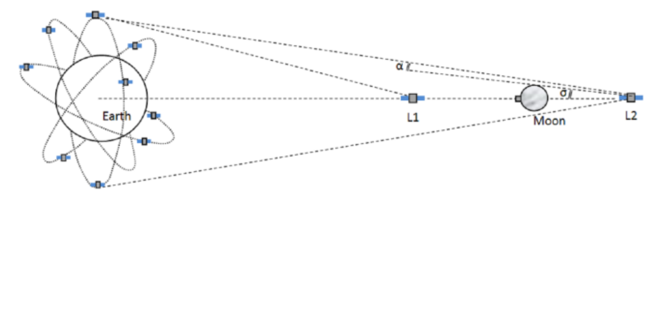

Fig. 3 The visibility of GNSS sources from Lagrange point L2 is limited due to Moon mask but definitely attained (sketch not to scale)

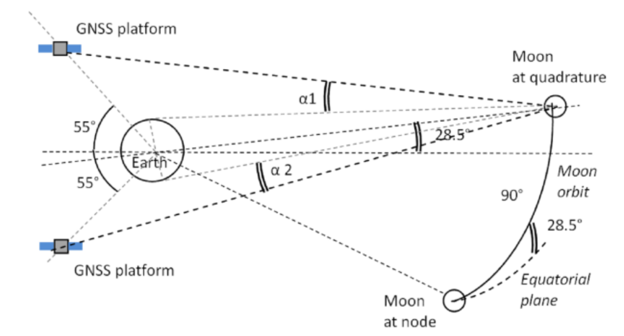

Fig. 4 GNSS visibility geometries with the Moon at quadrature and at the node point of the orbit

3 Receiver Requirements: Architecture and Algorithms

3.1 Acquisition

The acquisition process aims at coarsely estimating both code delay and Doppler frequency of the received signal, and therefore represents the first step towards signal tracking and message content recovery. For that purpose, the signal is correlated with different replica, each generated with the code and Doppler hypotheses to be tested. The energy of the correlator is then compared to a threshold which is set according to the requirement for the probability of false alarm (PFA), i.e. false detection of the code phase. In the study, the first step aimed at evaluating the exact dwell time structure and especially the required coherent integration time needed to fulfil both the probabilities of missed detection and of false alarm. For the targeted carrier to noise density ratio levels as low as 10 dBHz, the analyses rapidly confirmed that the coherent integration time needs to be much longer than the usual values applied for terrestrial applications in order to avoid prohibitive squaring losses caused by the non-coherent summations. Fig. 5 presents the probability of detection (PD) as function of the C/N_0 for different options of the coherent integration time and considering 50 non-coherent summations for a PFA of 1 E-3. Here C corresponds to the aggregate carrier power of the E5 signal using AltBOC modulation. The acquisition is performed with both Galileo E5 a-Q/b-Q pilot signals. The budget for the overall losses covers 6 dB for the single pilot component ‘extraction’, 1 dB (resp. 2 dB) for the code (resp. Doppler) misalignment losses and 2 dB for additional losses as cable, filtering, etc. Hence, a reasonable working point for the coherent integration time is 500 ms which will be used for the block averaging pre-processing (BAP), as explained later. Considering 50 non-coherent summations yields a dwell time of 25 s, a value which will strongly impact the selection of the acquisition architecture. Furthermore, a direct consequence of the longer coherent integration time is the smaller Doppler bin width necessary to keep the Doppler misalignment losses smaller than 2 dB. Extending the coherent time over the 20 ms bit transitions of the GPS C/A signal could be achieved, for example with a brute force approach (testing all $2^{500/20}$ combinations) or with a wipe-off of the data provided by a third channel. Now, in the study focus has been given to the acquisition of the Galileo E5 a-Q/b-Q and E1 C data less signals to demonstrate the technological feasibility. For such signals extending the integration up to 500 ms is eased by the presence of known secondary codes with a periodicity of 100 ms. Once the dwell time structure and value is known, the second step aims at the selection of the most appropriate acquisition architecture, as a trade-off between the mean time to acquire and the hardware resources.

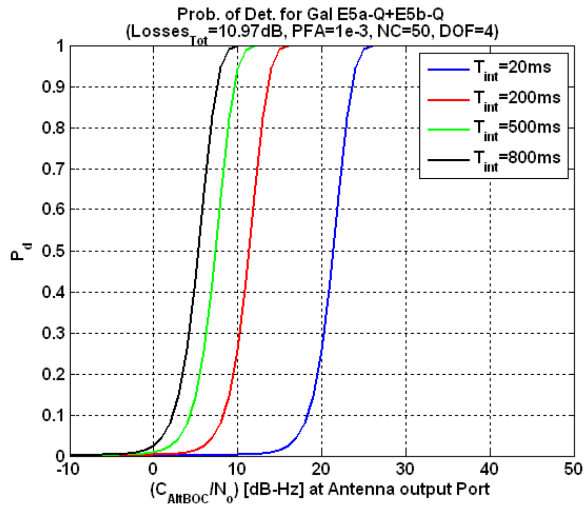

Fig. 5 Influence of coherent integration time on PD at low C/N0

The pros and cons for the three main categories of acquisition architectures, namely the active correlator, the passive matched filter and finally the time-frequency ('T-F') search based on FFT per code/Doppler block have been evaluated. In the active acquisition, a new segment of received signal samples is correlated each time with the new replica actualised with new code and Doppler hypotheses and tested in that way serially. This slows the acquisition time, but ensures independency of the successive tests and the first crossing of the detection threshold that leads to an acquisition 'hit'. In the case of the passive matched filter, the received signal is fed to a tapped filter whose taps match the spreading sequence chip polarity so that each code hypothesis is tested for every entering sample, thus accelerating the acquisition, but increasing strongly the number of operations per second. This leads to a partial dependency between successive tests. For both options an FFT can be applied to accelerate the Doppler search as described in [7]. Finally the T-F FFT search offers full parallelism (and full dependency) of the tested hypotheses within each block. A metric can then be built as ratio between the first and the second peak of the cross-ambiguity function (CAF) as evaluated with the FFT. This metric is compared to a threshold to declare the acquisition hit, as depicted in Fig. 12. In the analysis the T-F FFT search was retained on one side because many code/Doppler hypotheses can be tested almost simultaneously with a relative limited hardware impact on signal processing (DSP), and on the other side because a similar solution relying on FFT could be adopted for a signal tracking so that with a seamless transition between acquisition and tracking the uncertainty region could simply be 'narrowed'.

If the contribution of the satellite motion to the code and Doppler uncertainty can significantly be reduced with external aiding, this effect is not the case with the contribution from the clock in the receiver. Here two different types of chip scale clocks were considered for a benchmark: a caesium clock with an Allan deviation (Adev) of 1.5 E-11 s/s and an ultra-stable quartz oscillator with 4.4 E-6 s/s, both having the same power consumption of 120 mW [8]. By considering the longest period of non-visibility, T_{NV}, equal to 40 min, it is possible to determine the additional code and Doppler uncertainty due to the clock instability following the methods in [7] and summarised in the following table for the L1 band (f_{L1}=1575.45 MHz). Hence for a quartz oscillator, the frequency can span up to 7 kHz. These results highlight that reducing as much as possible the code/Doppler uncertainty region with external aiding makes only sense in combination with a stable local oscillator (Tab. 2).

Tab. 2 Impact of Local Oscillator Instability onto Search Space

Clock	**Adev[s/s] @40 min** $\sigma_{Adev,40\ min}$	**Frequ.uncert. span [Hz]** $\sigma_{Adev} \times \underline{f_{L1}}$	**Code uncert. span [s]:** $\sigma_{Adev} \times \underline{T_{NV}}$
Caesium SA.45	1.5 E-10	± 0.23	± 0.36 E-6
VFOV400 OCXO	4.4 E-6	± 6.9 E3	± 10 E-3

3.2 Tracking Architecture vs. Snapshot Approach

With the tracking architecture the receiver enters the tracking stage after the acquisition stage, once rough code phase and frequency are estimated. Now the tracking follows the dynamics of the signal, decoding the navigation messages and estimating pseudoranges. The requirements put on the GNSS receiver are very challenging both for the acquisition stage and the tracking. The very low C/N_0 caused by the large distances from the GNSS satellites imposes stringent requirements on the receiver design especially for the tracking function [4], [9]. Different choices exist about the signal tracking, mainly between the two main approaches:

- Closed loop architectures mainly based on non-linear estimation techniques. The resulting performance will be shown through semi-analytic simulations.
- Batch processing also known as snapshot techniques or open loop architectures, the strength of this technique will be further discussed.

A first consideration was a sequential processing approach with an estimation methodology using a Kalman filter with a non-linear implementation where code, carrier and frequency errors of the first correlation stage are used as a state vector that the filter has to estimate. In the non-linear implementation the In-Phase and Quadrature components are used as measurements for the estimation iteration. Then the estimated output is used as a direct feedback to the local signal generator or as the input for a control law [10].

The ability of the Kalman filter follows the dynamics of the incoming signal, therefore the inherent reduction of the noise together with the direct discrete time implementation, should allow to extend the coherent integration time in a more flexible way with respect to the classic phase lock loop approach [11], [12] avoiding loop stability problems due to the limitation on the loop bandwidth/coherent time product [9]. Two different non-linear techniques were implemented the Extended Kalman Filter (EKF) and Unscented Kalman Filer (UKF). The difference is in the necessity to linearize the measurement equations in the first technique while the UKF allows avoiding the linearization of the measurement model, providing more flexibility. The process is represented by a linear model [10]. The simulation task was performed following the well-known semi-analytic approach, an example of which can be found in [13].

The basic approach was to simulate the I and Q components with an analytic model, taking into account the most important effects on the code delay, phase error, frequency error and acceleration contribution. The simulated I and Q components were then fed as input to the tracking algorithms, in order to perform the estimation of the code and carrier state parameters; the main difference with the usual approach being that both code and phase tracking loops are simulated. The model used for the simulation assumes that the signal is normalized with respect to the noise on I and Q components and thus has a constant amplitude. The simulations were carried out considering different C/N_0 values going from 40 dBHz to 15 dBHz using the GPS L1 C/A signal. This is the considered limit for the stability of the tracking loop. The performance was analysed in terms of jitter for phase (in degree) and tracking error (in meters). The performance was also compared to the theoretical one of a classic 3^{rd} order PLL/DLL with coherent discriminators. This is representative of a linear tracking with coherent discriminator provided that the control loop can reach stability given the potential high loop bandwidth – coherent integration time (B.T) product. The formulas are valid only for small tracking errors or equivalently for high C/N_0. The jitter obtained from the actual error has been obtained by evaluating the standard deviation of the code phase error. Usually for high C/N_0 values a good agreement between theoretical and simulation results is found. However, for C/N_0 lower than 22 dBHz theoretical and simulation results start diverging [14]. This corresponds to C/N_0 values after which the efficiency of the Kalman approach can be well understood. For such low C/N_0 values the loop is no longer working in the linear region of the discriminator input-output function. Thus, the theoretical model is unable to capture the behaviour of the loop that is losing lock. The integration period chosen for both EKF and UKF was 400 ms.

A batch estimator computes estimates of signal parameters based on a batch of correlator outputs employing parallel estimation techniques to improve the signal observability. Contrary to the sequential closed loop tracking, batch processing maintains an open loop tracking architecture [15]. The batch processing allows the use of all the techniques that can benefit from the use of long batch of data in case of low carrier to noise ratio extending essentially the integration time. Nevertheless even in the absence of data transitions, the extension of coherent integration time proportionally reduces the tolerable frequency error due to the 'Sinc' pattern in the smoothing of the signal after the accumulation and dump process.

A similar effect is given by the on-board clock (reference clock) jitter, that is seen by the receiver as a Doppler effect superimposed on the Doppler due to the movement of the receiver antenna and of the GNSS satellites. As a consequence the overall effect is to smooth the peak of the correlation function with a ‘Sinc’ pattern [11]. This is the main drawback of this technique with reference to the accuracy of the pseudorange estimation. It is also true that the overall accuracy of the positioning is affected by the very high DOP due to the large distance and not optimal configuration of the GNSS constellation. Finally main features of the batch processing approach are:

- Improved signal observability as compared to sequential processing;
- Capability of parallel computations (parallel correlation computations performed by using frequency/domain correlation techniques);
- Improved tracking robustness as compared to a closed loop sequential tracking; batch processing overcomes the motion dynamic constraints on the bandwidth and design of a closed loop tracking filter and its stability issues. Instead, the motion dynamic needs to be followed within a correlator bandwidth, which is inversely proportional to a correlation interval.

Moreover with INS integration it has been demonstrated that batch processing maintains consistent carrier phase tracking without the knowledge of navigation data bits for the carrier to noise ratio in the range from 15 to 18 dBHz [15].

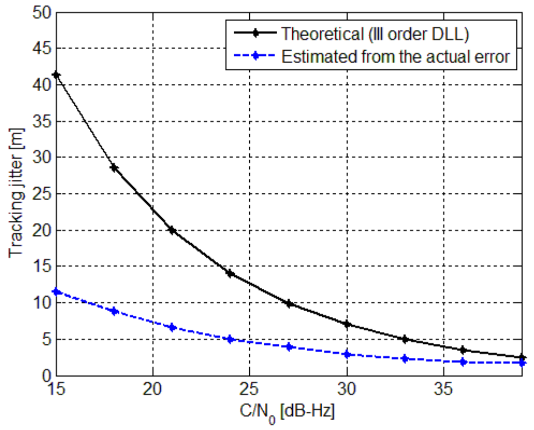

Fig. 6 Code tracking performance with UKF filter and 400 ms integration time

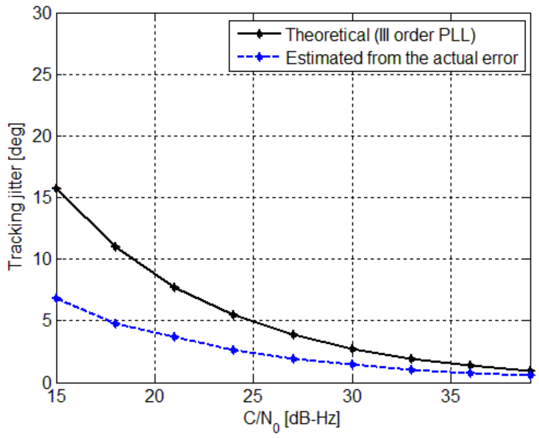

Fig. 7 : Phase tracking performance with UKF filter and 400 ms integration time

3.3 Configuration Parameters and Link Budget

The configuration parameters used for the link budget were selected to be as realistic as possible. This is the case of the equivalent isotropic radiated power (EIRP) patterns of the Galileo satellites. If the maturity of the GPS space segment, now implementing the Block III, offers rich and representative information regarding the GPS antenna and EIRP pattern (some based on real measurements available in diverse publications), for the Galileo system, currently in a deployment phase of the satellites with full operational capability (FOC) less information is available. Here the EIRP pattern for the aggregate E5 AltBOC signal is shown Fig. 8 as provided in [16]. Note that in our study we worked with the E5a and E5b Q components only where the power level is 3-4 dB lower (depending on the accounting for the filtering losses).

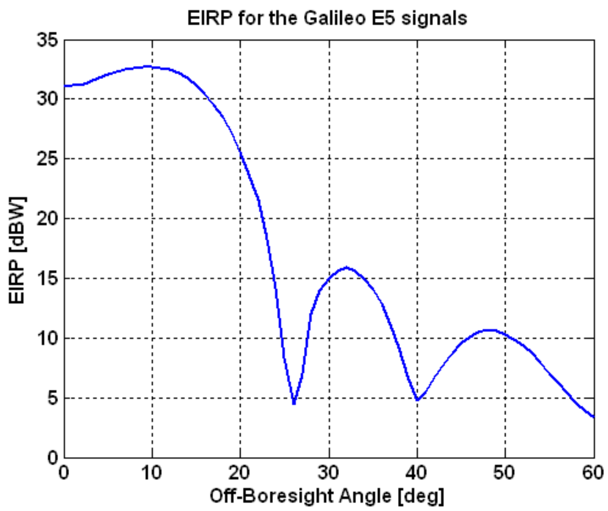

Fig. 8 Proposed antenna patterns for Galileo E5 signal (E5 a+b)

It must be underlined that an exact characterisation, with an accuracy of ±1 dB for large off-boresight angles of these EIRP patterns would be useless, due to the significant gain variations w.r.t. the azimuth [17], aging effects, or simply the type of Galileo satellite generation. Different options of active and passive receiver antennas (discrete, mechanical or electrical beam steering) were investigated to guarantee a large gain at reception, whatever the relative satellite attitude, w.r.t. the GNSS constellation. For example, some architectures considered up to six passive hemispherical antennas located each on a panel. A trade-off analyses considering power, mass and accommodation budgets led to retain an electronically steerable antenna as the best solution. Beam forming has the advantage to significantly improve the carrier to noise density ratio of all the tracked satellite links, but will make the receiver architecture more complex. The beam-forming network provides the means to form the reception beam of the array antenna towards the direction of the target satellite. The process is based on the weighting of the received signal samples of each individual array element where the pointing direction is dependent on complex excitation coefficients (for amplitude and phase). As the pointing varies with the time, these excitation coefficients will vary accordingly. Several configurations of beam forming were considered, either of spherical or planar shape, with varying number of elements. The following Fig. 9 represents the retained antenna pattern and corresponds with a spherical antenna of 20 elements and would ensure an antenna gain of 13 dBi.

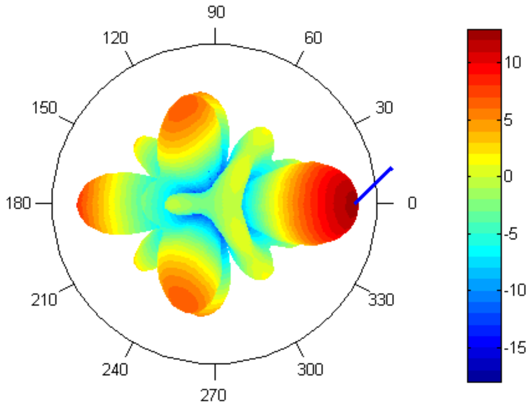

Fig. 9 Beam pattern of an antenna array with 20 elements (60 degree elevation, 0 degree azimuth)

For the lunar rover we suggested a 7 element planar antenna which is considered a very mature technology for ground application and will probably be used in the coming years in the aeronautical domain so that this technology should be mature for the time of a Moon mission. Tab. 3 compares the two suggested antenna types.

Finally Tab. 4 provides a typical loss budget applied to the Galileo E5 a-Q/b-Q. Here, the filtering losses cover the extraction of the BPSK (10) signals from the E5 aggregate signal. The correlation losses correspond to the extraction of the pilot signals, E5 a-Q/b-Q from the pilot and data signal E5 a/b. The additional losses include the filtering losses due to the reduced receiver bandwidth w.r.t. full transmit signal bandwidth, the product signals, implementation losses and cable losses:

Based on the former configuration parameters at tx and rx sides, dynamical link budgets have been calculated. Fig. 10 presents the C/N_o distribution (upper figures) as well as the cumulative distribution (lower figure) for the E5 a-Q or E5 b-Q processed individually, and the (coherently) combined E5 a-Q and E5 b-Q pilot signals at the correlator output. Here the worst case scenario is considered, when the spacecraft is in orbit around the Moon. Finally, for the aggregate E5 a-Q/b-Q signals, a value of 10 dBHz was retained as a working point for the receiver performance, knowing that about 80 % of the C/N_0 values are larger than this value. Note that the lower C/N_0 values in the figure correspond to the 'zeros' of the EIRP patterns or 'tertiary lobes' of the transmitting antenna pattern.

Tab. 3 Beam Forming Options

Note	Spacecraft	Moon rover
Algorithm	MPDR adaptive algorithm	MPDR adaptive algorithm
Number of elements	20	7
Expected Gain	13 dB	7 dB
Antenna form	spherical	planar
Number of antenna required	2 antenna required (1 on each side panel)	1
Complexity	Very challenging technology as the 2 antennas need to be perfectly synchronized. Moreover, this type of antenna is only tested as a prototype on ground. A considerable effort is foreseen to make this technology mature for the Moon mission.	Medium. This technology is very mature for ground application and will probably be used in the coming years in the aeronautical domain. This technology should be mature for a Moon mission in the future.

Tab. 4 Loss Budget for Galileo E5 a-Q/b-Q

Loss type vs. loss budget for	Galileo E5 a-Q/b-Q
Filtering losses	3 dB
Correlation losses for pilot signal	3 dB
Additional losses	2 dB

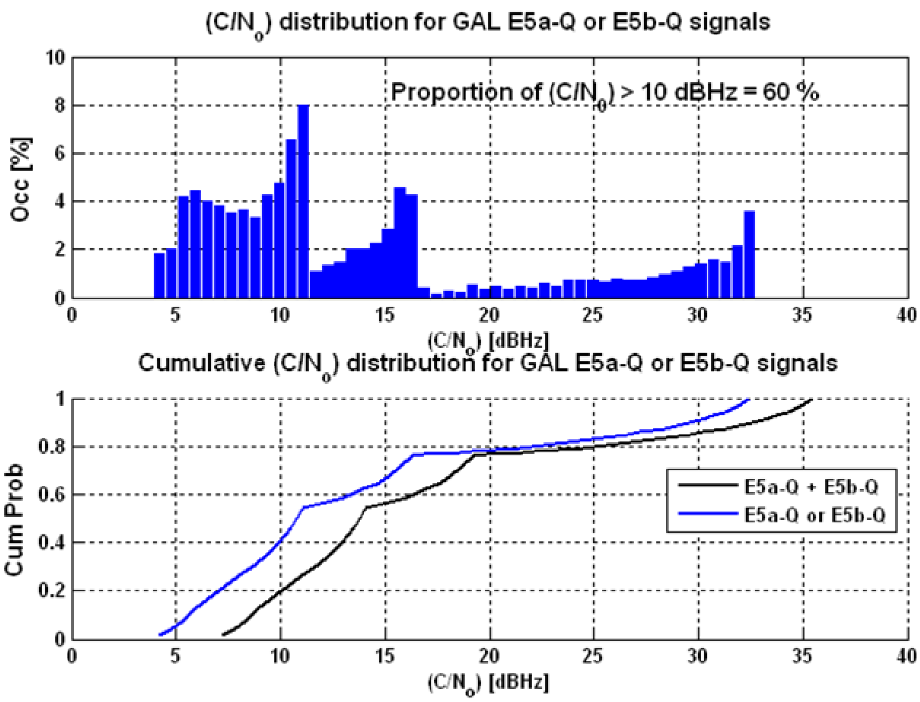

Fig. 10 Distribution of the C/N_0 for the single (a or b) and aggregate (a + b) E5 a-Q/b-Q signals for a Moon orbit

4 Receiver: Proof of Concept (POC)

4.1 Software Simulation

As a result of the above analysis and simulations we adopted the concept of the snapshot receiver with repeated signal acquisitions instead of the conventional signal tracking loop. During the various phases of the Moon mission much information about the state of the spacecraft and GNSS constellation is available in advance. In our software simulation we pre-calculated the kinematic states of the GNSS sources in an orbit propagator as well as the kinematic states of the spacecraft along its trajectory during representative phases of a Moon mission. With the internal representation of the spacecraft trajectory, sparse updates of the constellation information and the coarse spacecraft position it appears feasible to waive the decoding of the navigation messages. Instead we rely on the more robust acquisition of the secondary codes of the data less pilot channels of the E1 C and E5 a-Q/b-Q signals. The aiding information is initially provided also updated by the ground station. During normal operation the receiver obtains the coarse position aiding from loose coupling and feedback from the INS part as explained in the following chapters. In order to not loose accuracy over time also periodical feedback of the spacecraft position to the ground station is mandatory but can be assumed reasonable for a spacecraft.

4.2 Scenario Files

The software simulation uses scenario files for six different Moon mission types to generate the signal conditions of a GNSS receiver simulation. We used Matlab for all parts of the simulation and off-line processing of the test signals. We also reduced search spaces in the receiver simulation where possible in order to save processing time, i.e. we knew from the constellation and scenario simulation about the expected visibility of the GNSS sources and their carrier to noise ratios. As explained earlier we chose 10 dBHz as threshold of visibility of the carrier to noise power (per unit bandwidth), i.e. we ignored all weaker signals below this threshold. We chose an arbitrarily higher threshold of 15 dBHz for the case of the Moon transfer trajectory because of the larger number of visible sources resulting from the higher signal levels.

4.3 Signal Generation

We implemented a signal generation block for the three signals as a part of the proof of concept software. The purpose of the synthetic generation of the test signals was twofold: to be able to condition the test signals according to their simulated environment, that is to add Gaussian noise to achieve the C/N_0, and to apply Doppler shifts as would be expected from the service volume. The second purpose was to be able to exactly verify the success of the signal acquisition by comparison of the code phase from the signal generation with the resultant output. We started with generation and test acquisition of the standard GPS L1 C/A signal and coherent integration over the duration of one data bit (20 ms). Following the coherent integration we perform block averaging pre-processing (BAP), which was first described in [18]. The data blocks are then non-coherently combined for the desired signal length of up to 10s. The synchronous adding and averaging of the signal blocks requires the detection or knowledge from the aiding about the timing of the bit transitions. Confirming the analysis about signal thresholds we also found that coherent integration times of about 500 ms followed by non-coherent signal integration of up to 10 s would be required to achieve the required signal threshold of 10 dBHz. This led to the concept of using the full tiered codes of the Galileo E1 C and E5 a/Q-b/Q services with their data less pilot channels. For our proof of concept simulation we showed that for all simulated mission phases the visibility of GNSS sources was equal or larger than 4 satellites, being therefor sufficient to calculate the position fix. The GNSS blockage by the Moon mask would require the supplement by the INS part during this phase as well as during the descent phase where the long signal integration time and possible spikes in the Doppler would render the GNSS reception unreliable.

Tiered codes consist of a long primary code with high frequency that is XOR modulated with the short secondary code of low frequency. Thereby one bit of the secondary code corresponds to a full period of the primary code. Using these secondary codes allows the coherent integration of long signal periods, limited only by the change in Doppler shift and code delay which would result in a 'smeared' average of the correlation peak (a signal smoothing according to a ‘Sinc’ pattern). Another disadvantage of long coherent integration periods is the fact that the method acts as a frequency selective low pass filter with a zero crossing bandwidth of 2/L kHz with L being the number of accumulated 1 ms periods [18]. The effect of the low pass filtering can be overcome by an additional frequency search loop in the acquisition routines but poses another argument for aiding with the Doppler frequency from the ground station and/or from the feedback of the INS module. As we did not decode navigation data messages in our approach we were also able to replace these data with random content in the data channels where required for the signal generation.

4.4 Aiding

Both the acquisition stage and PVT solution make use of simulated aiding signals that are tailored for Moon GNSS navigation. These aiding signals in the real scenario would be provided by the ground station and/or a propagator unit. In classical receiver architectures the computation of full pseudoranges is accomplished by comparing time information broadcast by the satellite ephemerides data that are included in the navigation messages respectively in the handover word (HOW). In our simulation the receiver measures a fractional submillisecond pseudorange and does not decode the time information. Anyhow, it is of utmost importance to provide an estimation of the position with an accuracy less than 1ms for L1 C/A signals to ensure the receiver position inside a sphere with 150 km radius. Very similar but due to the need for knowing the start of the secondary code an accuracy less than 4 ms for E1 C signals is required which relaxes the required precision to a sphere with a radius of 600 km (the corresponding accuracy required for the Galileo E5 a-Q/b-Q signals would is 1 ms/150 km as with the GPS L1 C/A due to the shorter time for one full code length). The measured fractional part combined with this position estimation yields to a reasonable solution. Due to the waiving of navigation messages for the benefit a more sensitive and robust signal acquisition we need the aiding information provided by a ground station and/or a propagator unit, comprising position, velocity and PRN of the transmitting GNSS sources as normally decoded in the ephemerides data. Also the receiver coarse position and kinematic state of the spacecraft along the mission trajectory is required. In our simulation we used a trajectory tailored for every orbit scenario with position and velocity information, i.e. kinematic state of all GNSS sources with a time resolution of 1s. With these inputs the PVT estimation is possible without further knowledge about the time of week (TOW) parameter as would be required with a classical pseudorange computation.

4.5 Block Diagram

The block diagram in Fig. 11 shows the scenario simulation implementing the snapshot receiver concept. We established scenario description files for the investigated orbits (TR, LO, L1, L2) to define the visibility of the GNSS sources, signal level (C/N_0) and Doppler characteristics. We generated the baseband test signals (GPS L1 C/A, Galileo E1 C and Galileo E5 a-Q/b-Q) offline with time slices according to the signal integration and fed them as input to the signal acquisition stage.

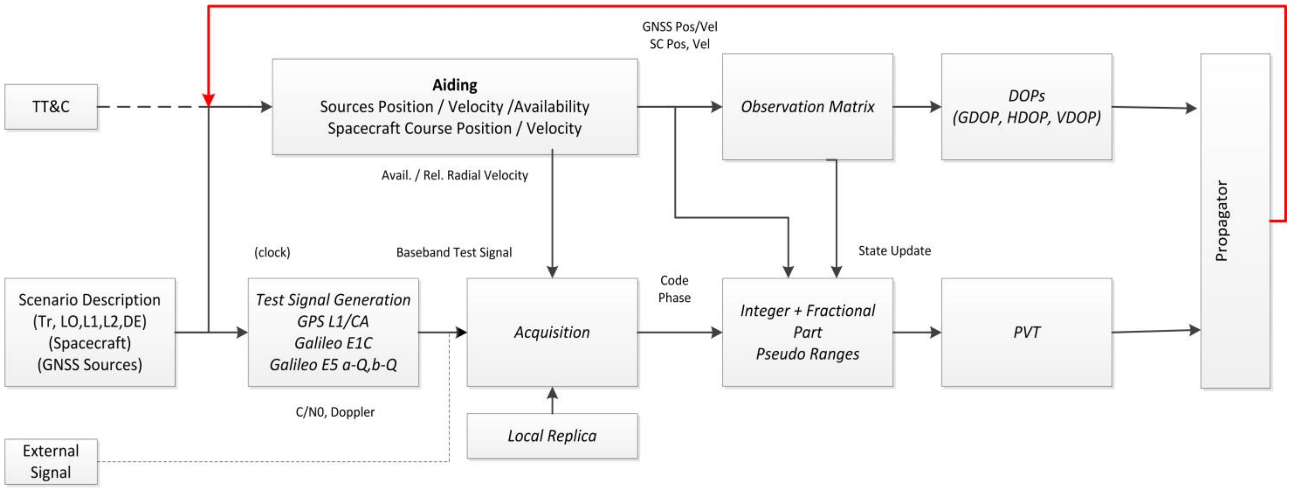

Fig. 11 Block diagram of the snapshot receiver with interface to the INS propagator

At this point also externally recorded signals could be input to the acquisition stage. The code phase of each test signal is acquired by correlation with the locally generated code replica. Success of the acquisition step is verified by comparison of the acquired code phase with the input signal. Would this information not be available the acquisition would be considered successful when the ratio of the main correlation peak to the second highest peak exceeds a predefined threshold. Fig. 12 shows examples of simulated Galileo E1C and E5 a-Q/b-Q pilot signals acquired at 12 dBHz.

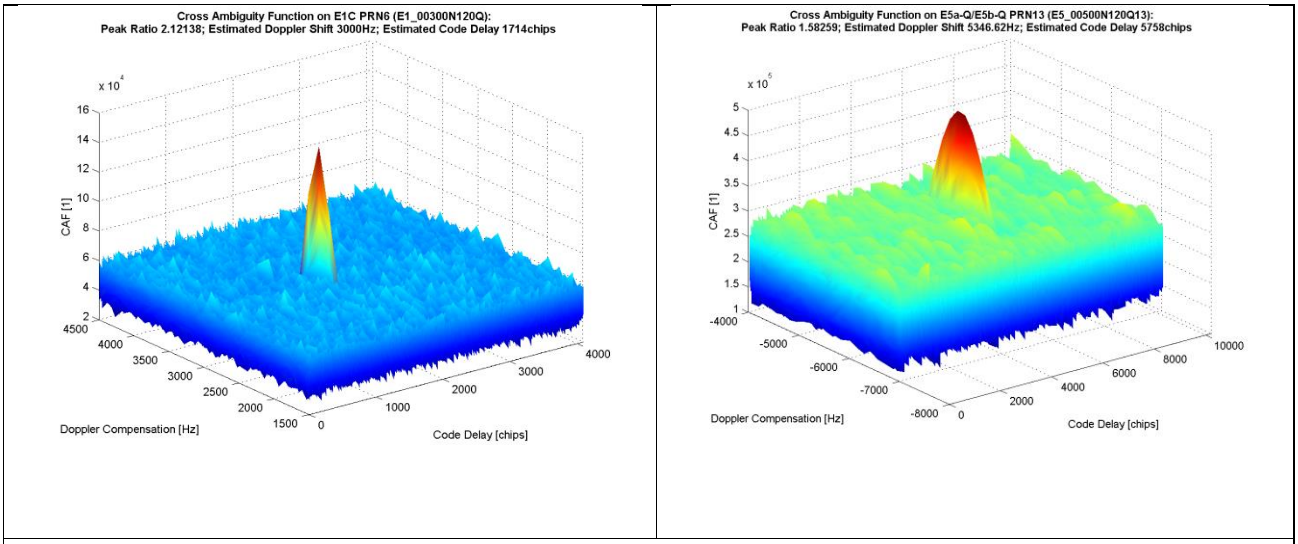

Fig. 12 Example CAF of simulated Galileo E1 C (left) and E5 a-Q/b-Q (right) pilot signals acquired at 12 dBHz

The code phase as the output of the acquisition step is fed to the PVT calculation stage which then combines the sub-ms fractional part of the pseudorange with the aiding information of the GNSS constellation and coarse information on position and kinematic state of the spacecraft. The aiding block forwards a list of the currently visible GNSS sources and their kinematic state plus the estimated coarse position and kinematic state of the spacecraft. The estimates about Doppler shift as well as integer and fractional pseudoranges are forwarded to the units:

- Acquisition stage
- Observation matrix
- PVT calculation

Without a conventional tracking loop it is especially important to utilise updates on the kinematic state of the spacecraft and/or constellation update to step the local carrier and to reduce the smoothing effect of a mismatched Doppler shift according to the sine cardinal frequency dependence of the acquisition process. This update of the Doppler shift can ideally be performed with every new coherent signal integration block.

4.6 PVT Calculation

PVT estimation can be segmented into several basic steps using the already mentioned aiding information of GNSS ephemerides data and the trajectory simulation of the spacecraft. First step is to determine the satellite position of all visible satellites via their pseudo random noise (PRN) numbers. As true position can only be simulated the decision has been made to use the simulated trajectory of the spacecraft as our 'true' reference position. To start with an a priori state the 'aiding' position was assumed with a random offset of a few kilometres to the 'true' trajectory. The aim of this simulation was to examine the correctness of the calculation. With these parameters we have a kinematic state of the visible satellites and an assumed a priori receiver position so that we now are able to estimate the pseudoranges. The unit vectors between the a priori position and the k^{th} satellite form the so called line-of-sight vectors and in further consequence, with at least 4 satellites in view, the observation or geometry matrix. Normally we are dealing with pseudorange measurements out of the acquisition stage to construct a true geometric range between the receiver and the satellite. Outputs of the acquisition stage are the sub-millisecond pseudoranges. In the next calculation step the millisecond integer ambiguity is resolved and the complete pseudorange is constructed using the technique of van Diggelen [19]:

A full reconstructed pseudorange is composed of an Integer $N^{(0)}$ plus a measured sub-millisecond pseudorange $z^{(0)}$, expressed in milliseconds. $N^{(0)}$ has to be assigned as a reference satellite by following this equation:

$$N^{(0)} = round(\hat{z}^{(0)} - z^{(0)}) \tag{1}$$

where $z^{(0)}$ is the actual fractional pseudorange measurement and $\hat{z}^{(0)}$ is the predicted full pseudorange. For all satellites we can now reconstruct all $N^{(k)}$:

$$N^{(k)} = round(N^{(0)} + \hat{z}^{(0)} - z^{(0)} + \left(\hat{r}^{(k)} - \delta_t^{(k)}\right) - (\hat{r}^{(0)} - \delta_t^{(0)})) \tag{2}$$

where $\hat{r}^{(k)}$ is the estimated geometric range from the a priori state, $\hat{r}^{(0)}$ is the actual geometric range and ${\delta_t}^{(k)}$ and ${\delta_t}^{(0)}$ are the satellite clock errors.

Last step in the PVT algorithm is the update of the a priori state to get the true receiver position. To solve for the receiver velocity and clock drift - using the least squares approach - the starting point is the pseudorange rate for each GNSS source by the following equation:

$$\dot{\rho}^k = [v^k - v_u] \cdot L_{unit}^k + \dot{b} + \dot{\varepsilon}_T^k \tag{3}$$

Where v^k is the velocity vector for satellite k, v_u is the velocity vector for the receiver, L^k is the line-of-sight unit vector, *b* is the clock drift and ε are error terms. Solving for the least squares estimate of and *b* yields to:

$$\begin{bmatrix} v_u \\ \dot{b} \end{bmatrix} = (G^T G)^{-1} G^T T \tag{4}$$

with

$$T = \dot{\rho}^k + G_k \begin{bmatrix} v^k \\ 0 \end{bmatrix} \tag{5}$$

We already described the calculation of the fractional pseudorange expressed in light milliseconds. These values

contain the real measurement part of the true range between the receiver and the satellite and can also be used

to aid the acquisition process by providing initial bit- and code delay (L1 C/A) and secondary code index (E1 C, E5 a-Q/b-Q) to narrow down the search window. The satellite-user geometry also influences the accuracy of the PVT solution and can be expressed as dilution of precision (DOP). This information is encoded in the geometry matrix G and depending on the dimension combined DOPs can be calculated:

$$H = (G^T G)^{-1} = \begin{bmatrix} H_{11} & - & - & - \\ - & H_{22} & - & - \\ - & - & H_{33} & - \\ - & - & - & H_{44} \end{bmatrix} \tag{6}$$

$$\begin{gathered} GDOP = \sqrt{H11 + H22 + H33 + H44} \\ PDOP = \sqrt{H11 + H22 + H33} \\ HDOP = \sqrt{H11 + H22} \end{gathered} \tag{7}$$

GDOP represents the total geometry DOP, PDOP the three-dimensional position DOP and HDOP the two-dimensional horizontal positioning DOP.

Aiding for the GNSS-based Position Fix: Previous discussion already introduced the need for some aiding from the ground station. This aiding is intended to provide the information usually granted by the navigation message (ephemerides, clock correction parameters, ionospheric model parameters) and required to compute the PVT solution. In fact, weak receiving condition deletes the chance to decode a message. However, it can be easily assessed that these data are valid for a long enough time, in the order of several hours: in fact, as an example, errors in the order of meters in the GPS sources' positions are based on messages that are several hours old. It means that very limited aiding, with content in the order of 1 kb, could be needed no more than twice a day to allow for the receiver to correctly compute the PVT solution. This aiding could be easily provided by a single ground station, without specific requirements on its longitude. Even if autonomy would not be - strictly speaking - complete, such a very limited aiding is a requirement far easier to match and less expensive with respect to the full ground based tracking of the mission.

5 Synergy with other Navigation Sensors

5.1 Inertial Navigation System

A strapdown inertial navigation system (SINS) is a self-contained autonomous navigation system. Measurements

of spacecraft angular rates and accelerations provided by inertial sensors (rate gyros and accelerometers) are used to track position and orientation of the spacecraft itself relative to a known starting set of position, velocity and orientation. A SINS includes the inertial measurement unit (IMU), inertial sensor assembly (ISA) and electronics for sensors calibration, thermal control, signal conditioning, etc.) and an on board navigation processor. The IMU typically contains three orthogonal rate-gyroscopes and three orthogonal accelerometers, mounted on a common base, measuring angular velocity and linear acceleration of the body reference frame (BRF) with respect to an inertial frame, expressed in the body frame (BF). By processing signals from these sensors it is possible to track the position and orientation of the hosting vehicle with respect to an inertial frame or a local navigation frame.

The form of the inertial navigation equations depends on which navigation frame (‘inertial’ frame, body fixed frame or local level frame) the navigation solution is expressed in. As far as the choice of inertial frames, some details shall be introduced here. Spacecraft navigation during coasting flight is performed by continuous measurements of position, velocity and time. The estimate of position and velocity is maintained in the navigation processor in non-rotating rectangular coordinates and is referenced to either the Earth or the Moon. An inertial non-rotating Earth-centered equatorial coordinate system is used when the vehicle is outside the lunar sphere of influence (Earth-centered, Earth Mean Equator and Equinox of J2000 – 'E-EME2000') [20]. In a strict sense, the word ‘inertial’, when used to describe a coordinate system, means that the coordinate system is unaccelerated. Thus, the only truly unaccelerated coordinate system in our solar system is a non-rotating coordinate frame centered at the solar system (barycenter). When the spacecraft enters the lunar sphere of influence, the center of the coordinates coincides with the center of the Moon. The ‘inertial’, non-rotating coordinate system is then the Moon-centered, Moon Mean Equator and IAU-node of epoch. The fundamental plane of the M-MEIAUE is the lunar mean equator and the fundamental x-axis is the IAU node of J2000 [20]. Following IAU/IAG conventions, the reference x-axis in an IAU-node of epoch coordinate system is defined as the cross product of the Earth’s mean rotational pole of J2000 with the Moon’s rotational north pole at the desired time. The z-axis is perpendicular to the mean equator of the Moon. When operating in proximity of the Moon a Moon-centered, Moon Mean Equator and Prime Meridian Body-fixed, rotating reference frame (M-MEPMD) is used. In this case, the x-axis of the coordinate frame is pointed in the direction of the Moon’s prime meridian and the z-axis (spin axis) is pointed in the direction of the Moon’s north pole. Computation of the inertial navigation solution is an iterative process, exploiting the solution of the previous iteration. The navigation solution must be initialized before the INS can operate; this is usually made with the aim of other external sources, such as star trackers as attitude sensors and GNSS as position data source.

IMU output quantities are measured in the spacecraft BRF. To keep track of orientation of the BF with respect to the inertial frame, the signals from the three rate gyroscopes must be integrated once. To track position, the three accelerometer signals are resolved into inertial coordinates using the known orientation; the inertial acceleration signals are then double-integrated to obtain position. The IMU provides measurements of the following quantities:

$$\boldsymbol{\omega}_{\mathrm{ib}}^{\mathrm{b}} = \left(\boldsymbol{\omega}_{\mathrm{xib}}^{\mathrm{b}}, \boldsymbol{\omega}_{\mathrm{yib}}^{\mathrm{b}}, \boldsymbol{\omega}_{\mathrm{zib}}^{\mathrm{b}}\right) \quad \mathbf{f}_{\mathrm{ib}}^{\mathrm{b}} = \left(\mathbf{f}_{\mathrm{xib}}^{\mathrm{b}}, \mathbf{f}_{\mathrm{yib}}^{\mathrm{b}}, \mathbf{f}_{\mathrm{zib}}^{\mathrm{b}}\right) \quad (8)$$

where $\boldsymbol{\omega}_{\mathrm{ib}}^{\mathrm{b}}$ and $\mathbf{f}_{\mathrm{ib}}^{\mathrm{b}}$ are, respectively, the vector of angular velocities of BF w.r.t. inertial frame, expressed in BF and the specific force (acceleration) vector of the BRF, expressed in the BRF itself. These measurements are used to keep track of the orientation of the BRF with respect to E-EME2000, and project specific forces on E-EME2000. To attain this, it is necessary to integrate the angular velocity components, where a representation of the spacecraft attitude must be selected between Euler angles, quaternions and direction cosines.

5.2 Mechanization Equations for Local Navigation

When approaching the Moon surface, i.e. during descent phase, and eventually for surface navigation, the navigation solution is expressed in a local level frame (ENU, lunar East, North and vertical upward geographic coordinate system) rather than in the inertial frame or lunar body fixed frame. The origin of the navigation frame coincides with the origin of the spacecraft body frame [21]. Basic SINS equations in local level frame (LLF) are:

$$\begin{bmatrix} \dot{\boldsymbol{r}}^l \\ \dot{\boldsymbol{v}}^l \\ \dot{R}_b^l \end{bmatrix} = \begin{bmatrix} D^{-1}\boldsymbol{v}^l \\ R_b^l f^b - \left(2\Omega_{im}^l + \Omega_{ml}^l\right)\boldsymbol{v}^l + \boldsymbol{g}^l \\ R_b^l(\Omega_{ib}^b - \Omega_{il}^b) \end{bmatrix} \qquad (9)$$

where the position vector of the spacecraft $\boldsymbol{r}^l = [\phi\ \lambda\ h\ ]^T$ is expressed in curvilinear coordinates in the Moon's body fixed frame (ϕ is the latitude, λ is the longitude and h is the altitude). The velocity vector $\boldsymbol{v}^l = [v_e\ v_n\ v_u]$ is in local frame, $v_e\ v_n\ v_u$ are the components in east, north, up directions respectively. The matrix D^{-1} transforms the velocity vector $\boldsymbol{v}^l = [v_e\ v_n\ v_u]$ from rectangular coordinates into curvilinear coordinates in lunar body fixed frame (M-MEPMD)

$$D^{-1} = \begin{bmatrix} 0 & \dfrac{1}{R_M + h} & 0 \\ 1/((R_M + h)\cos(\phi)) & 0 & 0 \\ 0 & 0 & 1 \end{bmatrix} \qquad (10)$$

where

$R_M = 1738.0\ \mathrm{km}$ is the radius of the Moon

R_b^l is the attitude transformation matrix from spacecraft BF to navigation frame (LLF), $\boldsymbol{f^b}$ is the output of the accelerometers expressed in spacecraft BF

$\boldsymbol{g}^l = \left[0\ 0\ 1.618 \frac{m}{s^2}\right]$ is the lunar gravity vector expressed in the navigation frame. Ω_{im}^l is the skew-symmetric matrix corresponding to the angular velocity vector ω_{im}^l of the Moon's fixed BF relative to the lunar inertial frame, expressed in the navigation frame; $\omega_{im}^l = [0\ \ \omega^m \cos(\phi)\ \ \omega^m \sin(\phi)]$ and $\omega^m = 2.66\ \ 10^{-6} \frac{rad}{s}$

Ω_{ml}^l is the skew-symmetric matrix corresponding to the angular velocity vector ω_{ml}^l of the navigation frame relative to the lunar body fixed frame, expressed in navigation frame; $\omega_{ml}^l = [-\dot{\phi}\ \ \dot{\lambda}\cos(\phi)\ \ \dot{\lambda}\sin(\phi)]$

$\Omega_{il}^b = R_l^b(\Omega_{im}^l + \Omega_{ml}^l)R_b^l$ is the skew-symmetric matrix corresponding to the angular velocity vector ω_{il}^b of the navigation frame relative to the lunar inertial frame, expressed in the spacecraft BF

Ω_{ib}^{b} is the skew-symmetric matrix corresponding to the angular velocity of the spacecraft BF relative to the lunar inertial frame, expressed in the spacecraft BF; the vector ω_{ib}^{b} is the output of the gyroscopes

The stochastic errors present on inertial sensors cause the subsequent numerical integrations of the measurements to exhibit an ever increasing variance. That is, when a gyro or accelerometer output is numerically integrated in a self-contained navigator, the variance in the resulting position and velocity outputs grows unbounded in time. This degradation of measurement accuracy propagates into the navigation solution at rates dependent on the integrity of the component sensors, the algorithms employed, and the duration of the un-aided navigation.

Errors from high-level inertial sensors, though very small, have to be accounted for in SINS implementation. Many error types can be detected from sensor functioning but as evidenced in both [11] and [12] the primary sources of errors in inertial sensors can be classified as:

- Bias (including a constant term and a time-drifting term);
- Noise, expressed by a random walk on the integrated measurement variable;
- Scale factor repeatability;
- Misalignment errors.

The sensor bias is defined as the average of the output, obtained during a specific period with fixed operational conditions, when the input is zero. The bias generally consists of:

- a bias offset or turn-on bias which is essentially the offset in the measurement and is constant over a single mission; it has deterministic nature and so can be determined by calibration procedure and easily compensated as an additive constant.
- a bias drift or in-run bias i.e. the rate at which the bias in the sensor accumulates with time; the bias drift has random nature since it is mainly due to flicker noise coming from electronics and so must be modelled as a stochastic process.

In terms of a mathematical model, the total bias can be described as a first-order process (Gauss-Markov process) of the following kind:

$$\dot{x} = -\beta x + \sqrt{(2\beta\sigma^2)}w \qquad (11)$$

where

β is the reciprocal of the correlation time of the process
w is zero-mean uncorrelated Gaussian noise vector of unit variance
σ^2 is the variance of the white noise associated with the random process

The sensor noise is a 'white noise' contribution to the signal which affects the measurement. It results from the sensor itself or from the other electronic equipment. Noise has random nature and cannot be removed using deterministic models, but can only be modelled stochastically. In inertial sensors, it is usually modelled as zero-mean white noise, i.e. it is considered to have a spectral density the same for all the frequencies of interest; in that case, specifications are usually provided by manufacturers in terms of random walk (RW) parameters, describing the average deviation or error that will occur from integrating the noise on sensor output signal. The relation between the RW parameter and the deviation on the the integrated variable is given by the equation below:

$$\sigma_{IV,wn} \cong \sigma_{RW}\sqrt{t - t_0} \qquad (12)$$

Where

$\sigma_{IV,wn}$ is the standard deviation on the integrated variable due to wideband noise,

σ_{RW} is the random walk process parameter, specified by manufacturers usually in terms of °/√h for gyros and µg/√h for accelerometers,

t is the current time,

t_0 is the sensor start-up time

The main issue with GNSS-aided navigation on Earth, i.e. the impossibility to obtain a GNSS solution because of poor visibility (number of satellites in sight < 4) has been partially solved in recent times with the aid of high quality inertial navigation systems. Hence GNSS/INS systems replace in higher and higher amount the classical GNSS-only based navigation systems. The main advantage of using the two methods together comes from their being complementary to another. The INS navigation solution is continuously available, providing navigation data even in the periods of GNSS visibility outage. The GNSS/INS integration is thus seen a fundamental support in the case of GNSS-aided mission to the Moon, where boundary conditions are yet different from those on Earth, since we find that

- GNSS no longer provide a long-term stability solution, as the spacecraft travels away from the Earth and DOP parameters progressively increase, reducing the accuracy of solution drastically
- INS cannot be used to detect gravitational accelerations hence it cannot provide the trajectory of the user spacecraft that is due to orbital dynamics (e.g. transfer, or low lunar orbit). Nonetheless it can be used to measure accelerations coming from other sources such as solar radiation pressure, engine thrusts etc.

GNSS no longer provide a long-term stability solution, as the spacecraft travels away from the Earth and DOP parameters progressively increase, reducing the accuracy of solution drastically. INS cannot be used to detect gravitational accelerations hence it cannot provide the trajectory of the user spacecraft that is due to orbital dynamics (e.g. transfer, or low lunar orbit). Nonetheless it can be used to measure accelerations coming from other sources such as solar radiation pressure, engine thrusts etc.

Furthermore, different levels of integration are feasible for GNSS/INS systems, among which the most used approaches are the following two:

- Loosely-coupled (LC) integration: raw GNSS data is processed first by a dedicated filter - KF or least square (LS) - to obtain PVT solution, then this is merged with INS output in another filter (usually a KF) to obtain the final estimate;
- Tightly-coupled (TC) integration: GNSS raw measurements are combined directly with INS data in a unique filter (again, a KF) with an augmented state vector. The integration is hence 'deeper'.

Comparing the two approaches it turns out that TC tends to yield slower processing speed due to the high amount of data processed by the 'centralized' filter, while LC is typically faster, being structured with two separate, lighter filter blocks [11]. If a LS filter is used to process GNSS data, process noise is not added twice, which would be the major drawback of this method. Furthermore, a loose integration behaves better in case of failure of one of the two sources. Schemes for the two integrated systems are shown in Fig. 11, where the dashed lines represent the closed-loop alternatives, which are adopted in order to increase the overall algorithm stability. In the final architecture the GNSS receiver obtains feedback from the output of the system, while the INS processor is reinitialized by GNSS PVT when available (a condition that cannot be satisfied behind the Moon). The INS is not reinitialized using the final output since this causes proven system instability.

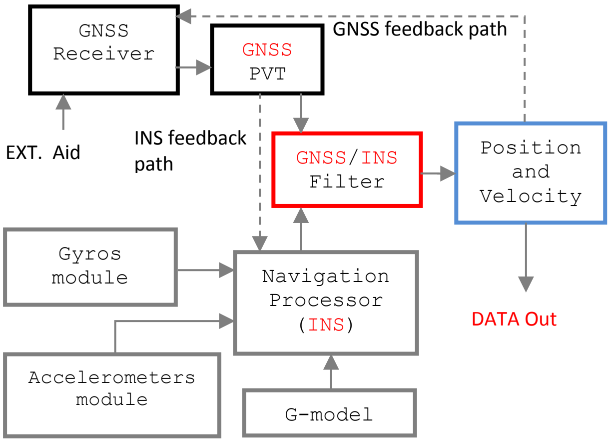

Fig. 13 GNSS/INS LC architecture with feedback loops

The choice of one architecture over the other has been established considering the following points:

- TC is conceived to use GNSS raw measurements (pseudo range, pseudo range rate and Doppler) and merge them to the centralized filter, hence it would not be able to provide an INS independent solution in case of GNSS total failure, as in case of low lunar orbit when behind the Moon (mask angle @ 200 km: 41.88°). In that case the number of available sources is zero, so that GNSS raw data cannot be extracted.
- During all other scenarios, even L2 point, assuming a 10 dBHz threshold for C/N_0, the visibility conditions are good (available sources > 4 for almost all the time), though DOPs become very high. The user spacecraft wouldn't in any case obtain advantage from using a TC architecture.
- The cost of TC is an increased algorithm complexity due to the TC 'centralized' filter, which is heavier in computational terms than the two separate filters in LC (one for GNSS PVT, and the other for GNSS and INS data merging) [9].

The role of the Kalman filtering in this context, is specifically to allow an INS-aided GNSS navigation, which is conceptually opposed to the 'classical' approach used on Earth navigation, that is, a GNSS-aided INS; the difference in the two types of problem is evident if one thinks how GNSS sources on Earth can be considered as a quasi-constant source with a nearly fixed accuracy (except under tunnels or urban canyons), which is absolutely not true for the Moon mission case. As explained above, the LC implementation is the only one to be reasonably considered for a feasibility analysis, so the current paragraph will give a better insight of the Kalman filter terms introduced in the simulations. For the current problem, we consider a reference solution provided by INS - which is available at a much higher rate - and correct it using periodically available GNSS data, that is, the term $\mathrm{H_k}\hat{\mathbf{x}}_{k|k-1}$ is substituted by INS-computed solution while the observation (innovation) vector is provided by GNSS PVT:

Prediction step

$$\begin{aligned} \hat{\mathbf{x}}_{k|k-1} &= \mathbf{x}_{INS,k|k-1} \\ P_{k|k-1} &= \phi_k P_{k-1|k-1} \phi_k^T + Q_k \end{aligned} \qquad (13)$$

Measurement update step (if GNSS is available)

$$\begin{aligned} K_k &= P_{k|k-1} H_k^T \left(H_k P_{k|k-1} H_k^T + R_k \right)^{-1} \\ \hat{\mathbf{X}}_{k|k} &= \hat{\mathbf{X}}_{k|k-1} + K_k \left(\mathbf{Y}_{GNSS,k} - H_k \hat{\mathbf{X}}_{k|k-1} \right) \\ P_{k|k} &= (I - K_k H_k) P_{k|k-1} \end{aligned} \tag{14}$$

Being $\hat{\mathbf{X}}_{GNSS/INS,k|k}$ the notation for the GNSS/INS filter output for time of simulation t_k. As evident, the position/velocity solution evaluated by INS is the predicted value, while the GNSS observable is the corrective term. The mapping matrix H_k can be suppressed in all cases being equal to identity matrix for all phases (where the state variables X, Y, Z, V_X, V_Y, V_Z are directly observable) except for descent, where local coordinates evaluated by INS are in terms of local longitude, latitude, and height. Following the LC approach for GNSS and INS integration, each time that a new GNSS observation is available, the INS solution is reinitialized; this increases as the solution stability, however this does not impact the noise on measurement, which is mainly due to electronic/thermal noise and cannot be eliminated but by re-starting the sensor through an off-on command, which would naturally be too time-demanding and in the long term would reduce the system performance. The following paragraphs will explore the design of the filter process models filter in both cases of free-space orbit and of local navigation (the latter valid only in case of descent and eventually of surface operation). The derivation of the dynamic matrices is based on the INS mechanization equations.

5.3 On-Board Navigator Software Simulation

This section addresses the overviews and simulation results of mission phases deemed as the most critical in terms of GNSS signal reception and/or processing. The definition of the selected scenarios essentially focuses on the following aspects:

- Orbital dynamics
- Spacecraft desired attitude
- Exploitable sensors/aiding systems
- Accuracy and availability of GNSS data

While as for the on-board propagator functionality, the following issues shall be dealt with:

- Type of non-linear Kalman filter (UKF/ EKF)
- Filter parameters values
- Integration of INS/GNSS/RDA aiding data
- Reduction of the uncertainty over navigation data

The phases of the Moon mission of major interest in this scope are resumed in the below table. For each of these scenarios, datasets are available as far as orbits and GNSS calculated solutions are available and have been exploited as inputs to the navigation processor software simulator.

Tab. 5 Identified Moon Mission Scenarios

Mission phase	Relevant issue
L2	Minimum carrier to noise ratio (only 10dBHz attainable)
Lunar Descent	Loosely-coupled integration may compromise the performance of GNSS aided INS during high dynamic manoeuvres
L1	Low carrier to noise ratio attainable at 15 dBHz
Equatorial Low Lunar Orbit	GNSS signal denied on the dark side of the Moon, re-acquisition of the signal exiting from outage
Transfer	High Doppler values expected (+60 kHz to -60 kHz), low to moderate C/N_0 expected (about 10 to 40 dBHz)

For all scenarios the following notes are valid:

- The time frame considered for each simulation amounts to 1800 s (1/2 hour trajectory) except for descent, with duration of 720 s;
- The GNSS update rate has been established to 30 s

All blocks and related sub-blocks of the INS software simulator have been developed in Matlab. The following Fig. 14 shows the functional structure:

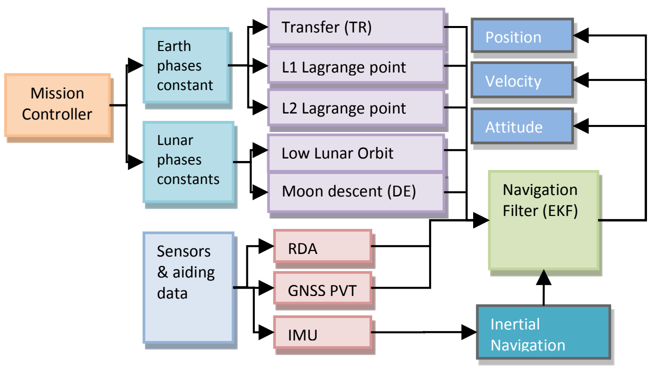

Fig. 14 INS software simulation

Note that, by a merely functional point of view, an orbit propagator (OP) module can be defined, including:

- the gravitational/gravity model of the main attracting body with which the INS software part is provided
- the filtering algorithm, Kalman-based, merging the PVT solution obtained from GNSS measurements (and/or eventually radar measurements) with inertial navigation equations solution to get a best estimate of the state, in the LC configuration. The KF algorithm is always running to get a

navigation solution, whatever the mission phase and whatever kind of data it is acquiring during that phase, and whether the GNSS solution is available or not. This will prove fundamental during the period of Moon shadowing, after which the re-acquisition of the GNSS signal on behalf of the spacecraft shall rely on the navigation solution computed by the orbital propagator along with the remaining aiding resources.

6 Orbit Determination and Tracking

Performance offered by the proposed technique needs to be compared with the ones provided by alternate, and actually pre-existing approaches, i.e. purposeful tracking from Earth based stations. Typical radio frequency measurements, together with communications from the Earth to spacecraft and from spacecraft to the Earth make use of selected (internationally agreed and protected) portions of S-band (2110-2120 MHz uplink and range 2290-2300 MHz downlink), X-band (7145-7190 MHz uplink and 8400-8450 MHz downlink), and Ka-band (34200-34700 MHz uplink and 31800-32300 MHz downlink). By combining different (one-way or two-ways, single or multiple receiving ground stations) it is possible to acquire extremely precise position/velocity measurement of the spacecraft. Tab. 6 reports data relevant to the ESA tracking network (from [22] and literature analysis). This accuracy usually exceeds the needs of the mission guidance task (as an example, the 'delta differential one-way range' (D-DOR) observable is only justified for radio science measurements, i.e. is related to the payload, and is relevant for tracking only in the special case of the determination of the end-of-life crash point on the lunar surface).

Tab. 6 Performance of Ground-based Tracking Techniques

Range	1 to 5 m
Range-rate (Doppler)	0.5 mm/s
Angle (D-DOR)	10 nrad

Even more important with respect to the present study, such a level of accuracy is clearly out of reach of the proposed GNSS based approach. But the real constraints limiting these ground-based tracking techniques are complexity, availability and cost. In fact the combination of the motion of the probe in lunar mission and the rotation of the Earth implies that a network of stations, at different longitudes, should be contracted. Moreover, as these stations, existing in limited number, are usually involved in tracking a large number of missions (in some case co-operating to standard launch and early operation phase (LEOP), otherwise tracking probes to inner planets or deep-space missions) their availability should be checked in (large) advance and should fit in tight schedule. As a result, cost of tracking is extremely high, to become a serious concern in the low thrust mission due to the long cruise phase. A solution is to limit the need for continuous tracking from Earth by allocating some autonomous guidance capabilities on board. Indeed, the rationale of the proposed GNSS-based approach is not related to the accuracy, which at the end is barely comparable with respect to the state-of-the-art, while more than sufficient for mission guidance. The real advantage stays in the support to almost autonomous operations, avoiding the burden of identifying and coordinating a number of ground stations, that also create strong constraints to mission operations schedule, and above all in the tracking cost, which is reduced by a fraction.

7 Testing of the POC

7.1 Service Volume and Acquisition Tests

The sw receiver should be able to perform successful GNSS acquisition within the range of expected parameters. Surveys and simulations led to the expected signal range of ± 60 kHz for the Doppler shift and a required target sensitivity of the receiver in the range 10 to 15 dBHz at the antenna output. With the above described Tx and Rx antenna characteristics we calculated the link budgets and signal conditions (C/N_0, Doppler) along selected sections of the expected mission trajectories. We generated test signals accordingly in steps of 1 dBHz/1 kHz and tested signal acquisition this way for 100 % of the service volume along the trajectories. The synthetic test signals covered the signal types GPS L1/CA and the data less pilot signals of Galileo E1C and E5 a-Q/b-Q (aggregate a+b channels). We used random content for the data channels were required for signal generation. The correct operation of the software was thoroughly verified with a total number of 986 / 801 / 856 signal generations and test acquisitions for the L1CA / E1 C / E5 a-Q/b-Q bands where only the L1/CA signals below 12 dBHz failed successful acquisition.

The service volume was tested for the coverage of the range of signal conditions during the testing. The software was also used to identify mission scenarios with critical signal conditions, i.e. scenario conditions with high Doppler shifts, periods with very low carrier to noise ratios (C/No) and combinations of these conditions. Fig. 15 shows an example of this testing where the number of occurrences of C/No vs. Doppler pairs are shown for an orbit at the Lagrange L1 point and signals in the L1/E1 frequency band. Grid resolution was 1 dBHz / 1 kHz.

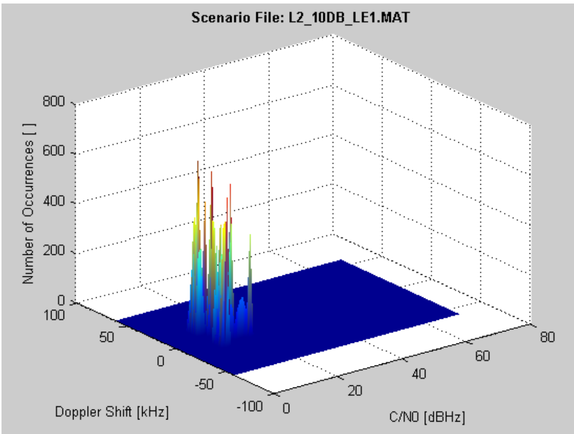

Fig. 15 Number of occurrences of Doppler - C/No pairs (L1 trajectory simulation with L1/E1 bands)

7.2 PVT Calculation

To achieve a proper result of the true position and velocity of a receiver, PVT calculation follows four steps of the navigation problem. Starting from the bottom with an a priori position, the composition of an observation matrix, the measurements of actual pseudoranges and recently the update of the a priori state forms the main part of the PVT solution program. Necessary input parameters for the calculation are the GNSS sources, comprising position and velocity of all satellites and the orbit scenario with the visibility, the Doppler and the C/N for each satellite. The simulated receiver trajectory serves on the one hand to check the results of the calculation and on the other hand to provide a further input as a starting point and an estimated a priori position. All simulation inputs for the different scenarios and thresholds are described in the Work Packages Reports. The corresponding data files are contained with the software. The output of the PVT solution is a matrix of data to be handed over to the propagator input and comprises the receiver positions, velocities, uncertainties and DOP's.

7.3 Selected Trajectory Points

7.3.1 Transfer Trajectory

During the transfer phase the signal levels can exceed 60 dBHz and appear with Doppler shifts of up to +/- 50 kHz. Because of the large number of visible sources the investigation has been limited to the higher signal threshold of 15 dBHz. Along the transfer orbit trajectory a random point at sec 290 has been chosen for the detailed investigation. Signal levels for the test point at the transfer were between 24 dBHz and 57 dBHz. At these high input levels it is expected that the acquisition / PVT calculation works well for all the investigated bands. The Doppler shift could be relatively high but no sudden changes are expected during this mission part. In the simulation Doppler shifts between – 43 kHz and +50 kHz were observed which is still well within the expected range of +/- 60 kHz. Coherent signal integration time was fixed with 500 ms, non-coherent integration time (signal duration) was reduced to between 0.4 s and 2 s to achieve a valid acquisition result but at the same time reduce calculation effort. The test acquisitions and PVT calculations

7.3.2 Lagrange Point L2

Signal levels for a test point at the Lagrange L2 point at second 103 in the simulation were between 10 dBHz (threshold) and about 22 dBHz. At these low input levels it is expected that the acquisition works well only for acquisition schemes with high coherent integration period as was fixed for the Galileo E1C and E5 a-Q/b-Q bands with 500 ms. Non-coherent integration time (signal duration) as an input to the signal generation was chosen between 8s and 10s in order to obtain a valid acquisition. The Doppler shift was observed between about -17 kHz and +17 kHz and is mainly attributed to the kinematics of the GNSS. All simulated test acquisitions of the Galileo E1C and E5 a-Q/b-Q at the test point performed correctly and detected the code delay that was input during the test signal generation. One of the seven visible sources for the GPS L1/CA signals was also correctly acquired at a signal level as low as 11 dBHz.

7.3.3 Descent

For our simulations we used a standard (synthetic) trajectory ('DE') as well as a profile after Bishop and Asimov that starts from a classical Apollo low-periselenium elliptical orbit and includes both a propelled (braking) phase and a ballistic phase (Looking at the overall conditions for the GNSS reception in terms of Doppler shifts and Carrier to Noise Ratio the signals appear predominately at a level of about 10 dBHz (and below), as well as Doppler shifts between about +20 kHz and -20 kHz are observed (LE1 bands). Under this aspect the characteristic signal ranges do not much differ between the two types of trajectories ('DE' vs. 'DEA17'). However, sudden changes in the Doppler shift can occur due to braking manoeuvres. Variations of the Doppler shift in the range of several Hz (absolute) as well as spikes and changing patterns in the Doppler rate can occur with Doppler rates in the order of several hundred Hz/s. In this case the concept of the snapshot receiver with long integration times and small bandwidths down to the order of 1-2 Hz clearly absolutely requires the INS coupling, as outages of the GNSS reception must be expected in such a condition. This is however where the INS propagator with its additional sensors namely the radar altimeter (RDA) fills in and justifies the concept. The simulations of the INS propagator include the 'descent' case and are detailed in the Work Package Reports.

7.4 Performances

7.4.1 GNSS

Without a priori on the satellite position, the Doppler uncertainty due to the geometry equals $\Delta f_D = 2 \cdot f_{D,max.}$ For the Lunar orbit, the expected Doppler range was -20/20 kHz, for the transfer phase up to -60/60 kHz was found in the simulations. Recent receiver technology allows the propagation of orbits for a prediction time of several days, allowing to host an orbit propagation algorithm capable of determining the satellite orbits with an error smaller than 50 m after 3 days, by using up-loaded ephemeris via the TT&C link of the mission satellite. Fig. 16 shows the corresponding prediction error [23].

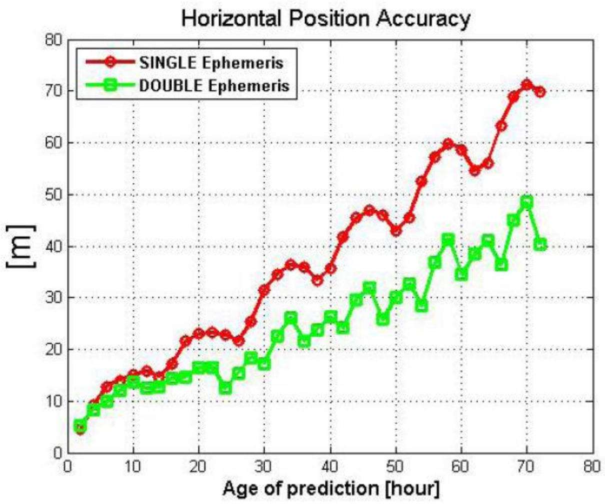

Fig. 16 Orbit prediction Error with an embedded orbit propagator in the receiver (from Mattos, 2008)

The satellite-user geometry influences the accuracy of the PVT solution. Some geometries will result in better accuracy than others. All information about Dilution of Precision is encoded in the observation matrix H. Out of this the following DOP values can be calculated:

$$H = (G^T G)^{-1} = \begin{bmatrix} H_{11} & - & - & - \\ - & H_{22} & - & - \\ - & - & H_{33} & - \\ - & - & - & H_{44} \end{bmatrix}$$

$$GDOP = \sqrt{H11 + H22 + H33 + H44}$$
$$PDOP = \sqrt{H11 + H22 + H33}$$
$$HDOP = \sqrt{H11 + H22}$$

To take into account a pseudorange error factor the value σ_{UERE} can be introduced into the formula above.

$$cov(dx) = (G^T G)^{-1} \sigma_{UERE}^2$$

$$cov(dx) = \begin{bmatrix} \sigma_x^2 & - & - & - \\ - & \sigma_y^2 & - & - \\ - & - & \sigma_z^2 & - \\ - & - & - & \sigma_t^2 \end{bmatrix}$$

Where:

$$GDOP = \sqrt{H11 + H22 + H33 + H44}$$

can be rearranged to:

$$\sqrt{\sigma_x^2 + \sigma_y^2 + \sigma_z^2 + \sigma_t^2} = GDOP \times \sigma_{UERE}$$

The following Tab. 7 shows typical contemporary sources expected for a σ_{UERE} budget in space:

Tab. 7 Typical expected contributions to σ_{UERE}

Error Source	Error (m)
Signal arrival C/A	± 3
Ephemeris errors	± 2.5
Satellite clock errors	± 2

7.4.2 Propagator / Estimator

The results of the software simulation of the Navigation Processor showed the following performances obtained for each of them (indicating with ε_{pos} the average of the maximum absolute error calculated as the difference between theoretical and estimated position, and with σ_{pos} the average standard deviation on the estimate itself):

Tab. 8 Performances of the Propagator / Estimator

Scenario	ε_{pos}	σ_{pos}	Notes
Transfer (D3 par 8.3)	150 m	800 m	
L1 Point (D3 par 8.4)	780 m	50 m on X, Z axes 1.1 km on Y axis	Partial non-availability of GNSS PVT in the L5/E5, 15 dB-Hz signal case
L2 Point (D3 par 8.4)	1.3 km	30 m on X, Z axes 2 km on Y axis	
Equatorial Moon orbit (D3 par 8.5)	7 km	60 m on X, Y axes 1.2 km on Z axis	Including Moon outage
Moon Descent (D3 par 8.6)	40 m	800 m on North and Down local directions 10 m on East direction	RDA aiding to be envisioned

8 Conclusions

In the Executive Summary Report and the detailed Work Package Reports we describe simulations for a space borne GNSS receiver that uses loose coupling to an inertial navigation system (INS). The receiver relies on the very low signal levels and partial visibility of the GNSS sources during various phases of a future lunar exploration mission. Within the expected service volume we simulate the expected orbital trajectories and kinematic states of a spacecraft to calculate GNSS availabilities and to generate test signals with the expected power levels and Doppler characteristics. Starting with the GPS L1 C/A signal we then concentrate on the data less pilot signals of the Galileo E1 C and Galileo E5 a/Q-b/Q services in order to achieve longer coherent integration times. We propose aiding with the a priori position of the spacecraft as well as with the expected Doppler shifts. Sparse position updates are required from the ground station as well as loose coupling with the INS. In conclusion, we expect that the exploitation of weak signals from existing and future GNSS could improve robustness and autonomy of lunar exploration missions.

9 References

[1] Bauer, F.H., et al., 'The GPS Space Service Volume', ION GNSS 2006.

[2] Miller, J.J., M.C. Moreau, 'Enabling a Fully Inter-operable GNSS Space Service Volume', International Committee on GNSS (ICG) Meeting, Beijing, 2012.

[3] Bate, R.R., D.D. Mueller, J.E. White, 'Fundamentals of Astrodynamics', Dover Publications, 1971.

[4] Palmerini, G.B., M. Sabatini, G. Perrotta, 'En route to the Moon using GNSS signals', Acta Astronautica, vol.64, n.4, pp. 467-483, 2009.

[5] Schoenmaekers, J., 'Post-launch Optimisation of the SMART-1 Low-thrust Trajectory to the Moon', Proceedings of the 18th International Symposium on Space Flight Dynamics (ESA SP-548). p.505-510, 2004.

[6] Koon, W.S., M.W. Lo, J.E. Marsden, S.D. Ross, 'Low Energy Transfer to the Moon', Celestial Mechanics and Dynamical Astronomy, vol.81, pp.63-73 (2001).

[7] Dafesh, P.A., J.K. Holmes 'Practical and theoretical Trade-offs of Active Parallel Correlator and Passive Matched Filter Acquisition Implementations', Proceedings of the IAIN World Congress and the 56th Annual Meeting of The Institute of Navigation, San Diego, June, 2000.

[8] Ucar, A., 'A Chip Scale Atomic Clock Driven Receiver for Multi-Constellation GNSS', The Journal of Navigation 2013.

[9] Rodriguez, F., G. B. Palmerini, 'Lunar Transfer Missions Navigation using GNSS Software Receivers', International Global Navigation Satellite Systems Society, IGNSS Symposium 2009, Qld, Australia, 1–3 December, 2009.

[10] O'Driscoll, C., G. Lachapelle, 'Comparison of Traditional and Kalman Filter Based Tracking Architectures', European Navigation Conference 2009 - Naples, Italy May 3-6, 2009.

[11] Pejman, L., Kazemi, 'Optimum Digital Filters for GNSS Tracking Loops', ION GNSS 2008, Session C5, Savannah, GA, 16-19 September 2008.

[12] Pejman, L., Kazemi, C. O'Driscoll, 'Comparison of Assisted and Stand-Alone Methods for Increasing Coherent Integration Time for Weak GPS Signal Tracking', ION GNSS 2008, Session C4, Savannah, GA, 16-19 September 2008.

[13] Borio, D., B. Pratibha, Anantharamu, G. Lachapelle, 'Semi-Analytic Simulations: An Extension to Unambiguous BOC Tracking', Proceedings of the 2010 International Technical Meeting of the Institute of Navigation, January 25 - 27, 2010.

[14] Pratibha, B., Anantharamu, D. Borio, G. Lachapelle, 'Pre-Filtering, Side-Peak Rejection and Mapping: Several Solutions for Unambiguous BOC Tracking', PLAN Group, Department of Geomatics Engineering, University of Calgary, GNSS 2009, Session F5, Savannah, GA, 22-25 September, 2009.

[15] van Graas, F., A. Soloviev, M. Uijt de Haag, S. Gunawardena, M. Braasch, ‘Comparison of Two Approaches for GNSS Receiver Algorithms: Batch Processing and Sequential Processing Considerations’, ION GNSS 13-16 September, 2005.

[16] Avanzi A., ‘Design and implementation of a novel multiconstallation FPGA-based dual frequency GNSS receiver for space applications’, 2012.

[17] Montesano, A., ‘Galileo System Navigation Antenna For Global Positioning’, 2007.

[18] Sahmoudi, M., M.G. Amin, R. Landry, ‘Acquisition of weak GNSS signals using a new block averaging pre-processing. In Position, Location and Navigation’ Symposium, IEEE/ION, pp. 1362–1372, 2008.

[19] van Diggelen, F. ‘A-GPS: Assisted GPS, GNSS, and SBAS’, Artech House 2009.

[20] Jet Propulsion Laboratory, JPL D-32296 ‘Lunar Constants and Models Document’, September 23, 2005.

[21] Groves, P.D., ‘Principles of GNSS, Inertial, and Multi-Sensor Integrated Navigation Systems (GNSS Technology and Applications)’, 2008.

[22] http://www.esa.int/Our_Activities/Operations/ Estrack_tracking_stations (access May 2015).

[23] Mattos, P.G., 'Hotstart Every Time - Compute the Ephemeris on the Mobile', ION GPS GNSS; 2; 822-829 Institute of Navigation; ION GNSS, 2008